ELSEVIER

www.elsevier.nl/locate/jorganchem

Journal of Organometallic Chemistry 592 (1999) 240–250

Journal of Organometallic Chemistry

$Ru(CH_3CN)_3Cl_3$, preparation and use as a mediator for the electrooxidation of hydrocarbons

L. Appelbaum [a], C. Heinrichs [b], J. Demtschuk [c], M. Michman [a,*], M. Oron [a], H.J. Schäfer [b,1], H. Schumann [c]

[a] *Department of Organic Chemistry, The Hebrew University of Jerusalem, 91904 Jerusalem, Israel*
[b] *Organisch-Chemisches Institut der Westfälischen Wilhelms Universität, Corrensstraße 40, D-48148 Münster, Germany*
[c] *Institut für Anorganische und Analytische Chemie, den Technische Universität Berlin, D-10623 Berlin, Germany*

Received 12 July 1999; accepted 9 September 1999

Abstract

Hydrogenation of ruthenium chloride in acetonitrile yields complexes of the type $Ru(CH_3CN)_nCl_{6-n}$ of which three are isolated ($n = 2, 3, 4$). Their formation is traced by voltammetry. $Ru(CH_3CN)_2Cl_4$ and $Ru(CH_3CN)_3Cl_3$ have been characterized by single-crystal X-ray diffraction. Voltammetry shows that $Ru(CH_3CN)_3Cl_3$ acts as a mediator for oxidation of cyclohexene, methylcyclohexene, 1-tetralol and tetralin. Its role in tetralin oxidation is illustrated by preparative scale electrolysis. The compounds $Ru(CH_3CN)_2Cl_4$ and $Ru(CH_3CN)_4Cl_2$ did not react with any of the mentioned hydrocarbons.

Keywords: Tris(acetonitrile)ruthenium trichloride; Electrocatalysis; Indirect electrooxidation; Tetralin; Tetralone

1. Introduction

Catalysis of electrochemical reactions by indirect electrolysis has two objectives: enhancing electron-transfer (ET) and controlling selectivity for desired products. Since electrochemical reactions are multi-step processes involving surface interaction, ET steps and homogeneous follow-up reactions, the effect of any prospective catalyst depends on its role in any of these stages. Locating the details of its functions is therefore essential for any methodical catalyst study. Aspects of electrocatalysis have been reviewed and discussed [1–4] and several recent works illustrate the variety of opportunities in this field [4,5].

Organometallic compounds and complexes often play an important role [4,5] where closely spaced oxidation states and spin multiplicity are essential for ET mediation and where aptitude in ligand exchange contributes to the control of selective reactions. Among these, $RuCl_3 \cdot 3H_2O$ has long been known as an ubiquitous homogeneous catalyst [6]. Recently, $RuCl_3 \cdot 3H_2O$ was found to be a catalyst in the electro-oxygenation of several olefins and aromatic compounds in acetonitrile [7]. We have found that it also enhances the reactions of aromatic radical-cations with water [8]. Further details concerning its effect are sought by probing the reactivity of $RuCl_3 \cdot 3H_2O$ with radical-cations [9] and by studying possible consequences of its chemistry in acetonitrile, as in this work.

$RuCl_3 \cdot 3H_2O$ has been described as a complex material that contains Ru(IV) species, Ru–O bonds and Ru–Cl bridged aggregates [10,11]. The nature of the catalytic entity is therefore not obvious. It is reasonable to expect that during prolonged reactions in acetonitrile some coordination of solvent takes place and may influence the catalytic process. Many possible conversions come to mind but very little solid knowledge is available on this point. The study of acetonitrile–ruthenium chloride compounds as possible catalysts is therefore a reasonable objective. The series of compounds, of the type RuL_nCl_{6-n} ($L = CH_3CN$, ArCN) and some of their corresponding ions have been studied extensively by Duff and Heath [12,13]. An almost linear

* Corresponding author.
E-mail address: michman@cc.huji.ac.il (M. Michman)
[1] Also corresponding author.

0022-328X/99/$ - see front matter
PII: S0022-328X(99)00532-X

effect of the ligands on the redox potentials was observed. Acetonitrile has a strong influence in increasing the redox potentials of the central ruthenium atom. Propositions of effects caused by exchanging chloride with acetonitrile have been made for other cases [14] and have been discussed by Duff and Heath for $Ru(CH_3CN)_nCl_{6-n}$ and $Ru(C_6H_5CN)_nCl_{6-n}$ on the basis of voltammetry, spectroscopy and calculation of Frontier orbital energies. Electrochemical transformation between members in the series has been observed and the pattern of electrode potentials and charge transfer data is systematically correlated to halide and nitrile ratios. This provides ground for their methodical study as catalysts. Bearing in mind the facile interconversion of members of this series under the conditions of electrochemical reactions, their preparation and structure need to be carefully controlled. As a feasible way to incorporate acetonitrile into ruthenium chloride we chose hydrogenation. Reduction in acetonitrile with H_2 over Pt on carbon black, has been reported to yield a stable, crystalline $Ru(CH_3CN)_4Cl_2$ (**1**) [15] whereas in methanol or DMF, hydrogenation of $RuCl_3{\cdot}3H_2O$ was reported to yield a complex 'blue solution', which acts as a catalyst mixture in several cases and consists of a mixture of reduced ruthenium compounds [16]. The difficulty in isolating such dissolved intermediates is obvious. Voltammetry was chosen in this work as the preferred method for following the formation of the acetonitrile complexes.

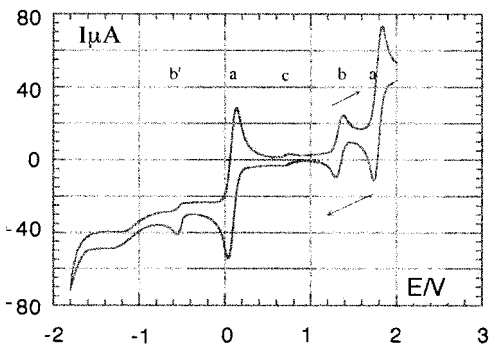

Fig. 1. CV of the complex mixture obtained from hydrogenation of $RuCl_3{\cdot}3H_2O$ on 5% Pt/C in CH_3CN. Sample: after 10 h reaction. Pt electrodes, Ag | AgCl | KCl reference, in 25 ml CH_3CN, 0.1 M TBAP. Scan rate 100 mV s^{-1} (from +2 to −1.8 V and back). Scanning is performed from a very positive potential value, to provide a clear and full picture. Scanning from another point gives the same information (cf. Figs. 3 and 4). CV at b is of $Ru(CH_3CN)_2Cl_4$ (**2**); b′ appears with b in the voltammetry of **2** but is of unexplained shape. CV at c is of $Ru(CH_3CN)_4Cl_2$ (**1**) and those marked a are of $Ru(CH_3CN)_3Cl_3$ (**3**). Only transition a at 1.84 V, is active as an ET catalyst.

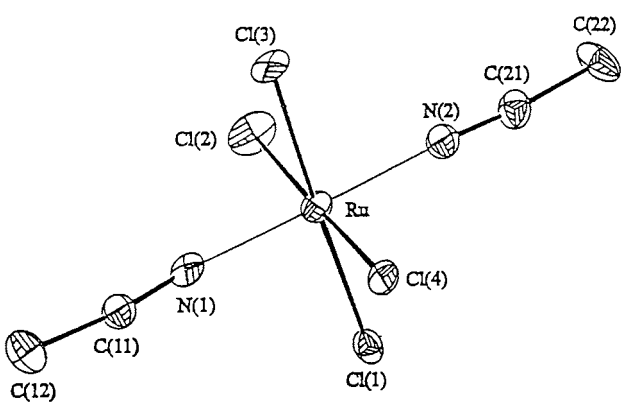

Fig. 2. ORTEP (k) plot of the molecular structure of **2**. Selected bond lengths (Å) and angles (°) with estimated S.D. values in parentheses: Ru–N(1) 2.024(7), Ru–N(2) 2.016(7), Ru–Cl(1) 2.338(7), Ru–Cl(2) 2.326(7), Ru–Cl(3) 2.368(6), Ru–Cl(4) 2.356(8), N(1)–Ru–N(2) 178(2), N(1)–Ru–Cl(1) 93.4(7), N(1)–Ru–Cl(2) 90.0(8), N(1)–Ru–Cl(3) 87.4(7), N(1)–Ru–Cl(4) 90.4(8), Cl(1)–Ru–Cl(2) 91.37(10), Cl(2)–Ru–Cl(3) 90.7(3), Cl(3)–Ru–Cl(4) 88.20(10), Cl(4)–Ru–Cl(1) 89.7(3).

2. Results and discussion

2.1. Complexes of $RuCl_3{\cdot}3H_2O$ with acetonitrile

The slow catalytic hydrogenation of $RuCl_3{\cdot}3H_2O$ was carried out in acetonitrile at 25°C and at ambient pressure. Within several hours (depending on catalyst activity), a precipitate of acetonitrile complexes was obtained (about 1.2 g from 1.5 g of $RuCl_3{\cdot}3H_2O$), in which **1**, $Ru(CH_3CN)_2Cl_4$ (**2**) and $[Ru(CH_3CN)_3Cl_3]$ (**3**), were identified. A continuing process of ligand exchange and reduction is involved and the composition of the precipitate changes in the course of reaction. The change is monitored by cyclic voltammetry (CV) at predetermined intervals. Whereas $RuCl_3{\cdot}3H_2O$ shows a complicated and blurred voltammogram of redox transitions, the reaction mixture gradually gives way to definite patterns among which are those of **1**, **2** and **3**. Fig. 1 illustrates the kind of CV obtained in the course of reaction. The reaction can be interrupted to facilitate isolation of specific compounds. $Ru(CH_3CN)_2Cl_4$ (**2**) forms early in the hydrogenation. From a precipitate collected at an early stage as judged by CV, when it contained mostly **2** and **3**, crystals of **2** (about 50 mg), were isolated. Compound **2** has the octahedral trans structure shown in Fig. 2. Crystals of **2** show a reversible CV at E_p^{oxid} 1350 mV, an irreversible reduction at −600 mV and a very small oxidation current at 0.0 (impurity) (Fig. 3). The reduction at −600 mV is of low current intensity compared with the redox at 1350 mV. It similarly shows in CV of powders containing **2**. We have no clear assignment for it.

Prolonged hydrogenation increases the concentration of $[Ru(CH_3CN)_3Cl_3]$ (**3**), in the precipitate. This compound has been separated by chromatography as a brick-red powder. It shows two reversible single-electron transfers at E_p^{oxid} 133 mV and at E_p^{oxid} 1840 mV (Fig. 4). Scanning in Fig. 4 starts at a negative potential (to Ag | AgCl), in order to give the complete picture.

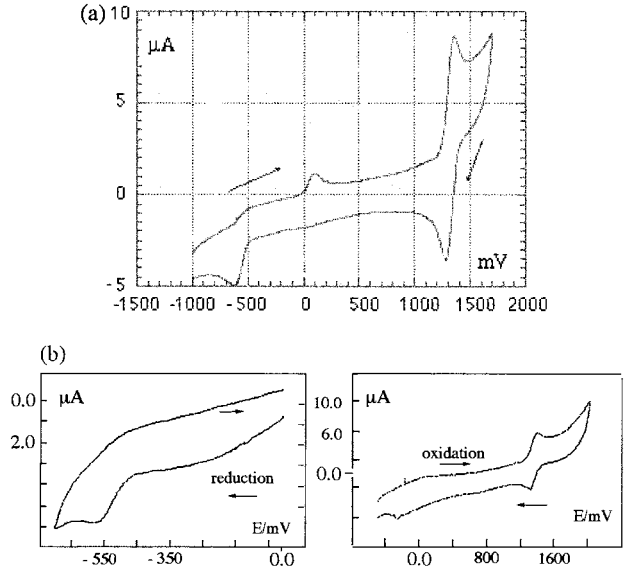

Fig. 3. (a) CV of isolated crystals of $Ru(CH_3CN)_2Cl_4$ (**2**). Scan rate 100 mV s^{-1}, 10^{-3} M of **2** in 25 ml CH_3CN, 0.1 M TBAP (impurity at 0.1 V). Scan of another sample, from $E=-1.0$ to $E=1.7$ V and return. (b) Scanning from $E=0.0$ to $E=-1.0$ V and separately from $E=0.0$ to $E=+2.0$ V shows the same reduction and oxidation patterns. The currents between 0.0 and −1 have no satisfactory explanation.

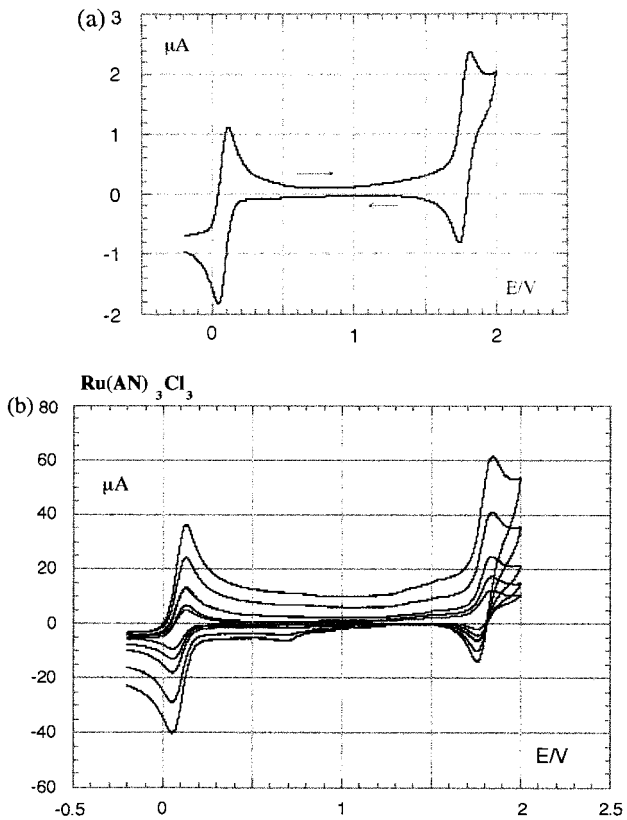

Fig. 4. (a) CV at 100 mV s^{-1} of $Ru(CH_3CN)_3Cl_3$ (**3**), 6.6×10^{-4} M in 25 ml CH_3CN, 0.1 M TBAP, after chromatography. (b) Steady state CV. Scan rate: 50, 100, 200, 500, 1000 mV s^{-1}. Scan direction: oxidation than reduction. Scanning in Fig. 4 starts at negative potential (to Ag | AgCl), in order to give the complete picture (see text).

The same curve features are retained when scans are started anywhere within the range shown, or run against a different reference ($Ag\,|\,AgBF_4$). (Compare for example Fig. 4 with Fig. 1.) From 1.5 g $RuCl_3\cdot3H_2O$, 1.1 g of clean **3** were obtained. Crystals of **3** as the octahedral mer isomer (Fig. 5) were grown from saturated solutions of the powder in CH_2Cl_2–ether. The crystals and the powder have identical CV.

The previously reported $Ru(CH_3CN)_4Cl_2$ (**1**) [14], is isolated as a yellow powder only after extensive hydrogenation or hydrogenation of **3**. It shows a single reversible redox transition at E_p^{oxid} 753 mV, identical to the CV of a sample of $Ru(CH_3CN)_4Cl_2$ prepared independently [17].

Hydrogenation obviously cleaves bonds like chloro-bridges in the ruthenium chloride structure and enables coordination of acetonitrile with ruthenium. Formation of **2** is unexpected. The yield — by a rough estimate from CV (re Fig. 1) — is around 10–15%. The simplest explanation is that some Ru(IV) is present in the original ruthenium chloride sample. This has been noted elsewhere [10]. Perhaps more complicated processes and certainly more products are involved. The present results concern the reaction that is summarized in Eq. (1):

Ruthenium–acetonitrile complexes in sequence of formation: **2**, **3**, **1**.

$$RuCl_3\cdot3H_2O + nCH_3CN \xrightarrow{[H_2]} \underset{\mathbf{2}}{Ru(CH_3CN)_2Cl_4} + \underset{\mathbf{3}}{Ru(CH_3CN)_3Cl_3} + \underset{\mathbf{1}}{Ru(CH_3CN)_4Cl_2} \quad (1)$$

Reversible CV and the steady-state CV over extended age, of the solids and of solutions show that all three compounds are stable in air and in acetonitrile with 0.1 M tetrabutylammonium perchlorate (TBAP) or $LiClO_4$ as electrolyte.

Compounds **1** and **2** were not involved in the catalysis discussed below and were not studied further in this work.

2.2. Structures

Crystals of **2** from CH_3CN–$CHCl_3$ and of **3** from CH_2Cl_2–ether were analyzed by X-ray diffraction. The unit cell of **2** contains two molecules of $Ru(CH_3CN)_2Cl_4$, two molecules of CH_3CN and two water molecules, resulting in $\{[Ru(CH_3CN)_2Cl_4][CH_3CN][H_2O]\}_2$, whereas that of **3** contains two molecules of $Ru(CH_3CN)_3Cl_3$ and four molecules of CH_3CN resulting in $\{[Ru(CH_3CN)_3Cl_3][CH_3CN]\}_2$. **2** crystallizes in the space group $P2_1$ and **3** in $P\bar{1}$, the difference may be caused by the presence of solvent molecules. **2** has a *trans*-octahedral coordination geometry with four Cl ligands in the equatorial positions and two CH_3CN ligands in the axial positions and the molecule is iso-

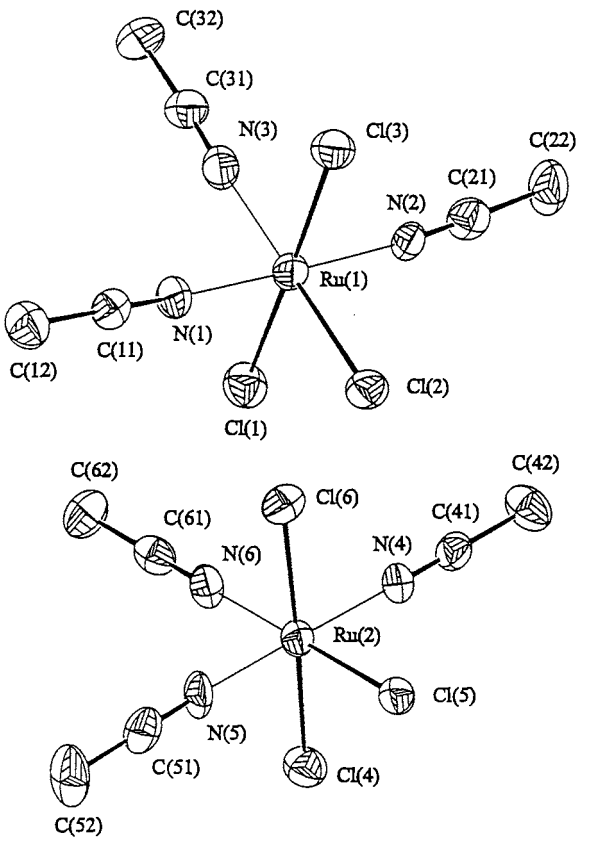

Fig. 5. ORTEP (k) plot of the molecular structure of **3**. Selected bond lengths (Å) and angles (°) with estimated S.D. values in parentheses: Ru(1)–N(1) 2.018(7), Ru(1)–N(2) 2.024(6), Ru(1)–N(3) 2.065(7), Ru(1)–Cl(1) 2.334(2), Ru(1)–Cl(2) 2.310(2), Ru(1)–Cl(3) 2.324(2), Ru(2)–N(4) 2.023(7), Ru(2)–N(5) 2.014(7), Ru(2)–N(6) 2.055(7), Ru(2)–Cl(4) 2.330(2), Ru(2)–Cl(5) 2.303(2), Ru(2)–Cl(6) 2.335(2), N(1)–Ru(1)–N(2) 178.2(2), N(1)–Ru(1)–Cl(1) 91.3(2), N(1)–Ru(1)–Cl(2) 89.2(2), N(1)–Ru(1)–Cl(3) 89.7(2), N(1)–Ru(1)–N(3) 90.3(2), N(3)–Ru(1)–Cl(2) 178.8(2), Cl(1)–Ru(1)–Cl(3) 176.31(8), N(4)–Ru(2)–N(5) 179.1(3), N(4)–Ru(2)–Cl(4) 90.3(2), N(4)–Ru(2)–Cl(5) 89.5(2), N(4)–Ru(2)–Cl(6) 89.3(2), N(4)–Ru(2)–N(6) 91.6(3), N(6)–Ru(2)–Cl(5) 178.7(2), Cl(4)–Ru(2)–Cl(6) 175.77(8).

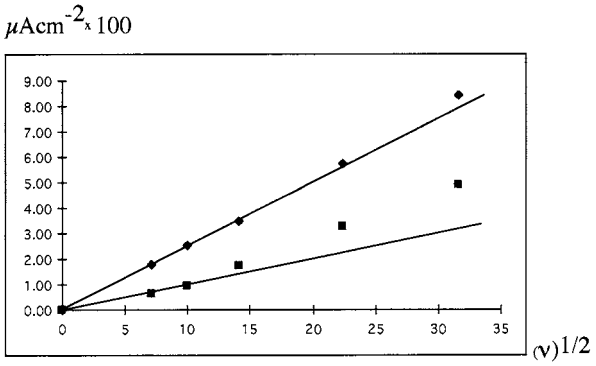

Fig. 6. Plot of anodic peak–current density: i_p^a cm^{-2} × 100, vs. $(v)^{1/2}$ of $Ru(AN)_3Cl_3$ (**3**) 6.6×10^{-4} M in acetonitrile. Lower line: CV at 133 mV; upper line CV at 1840 mV. Each scanned at 50, 100, 200, 500 and 1000 mV s^{-1}.

structural to the $[Ru(C_6H_5CN)_2Cl_4]^-$ anion [18]. Bond distances and angles are comparable. The average Ru–Cl distance of **2** (2.347 Å) is in the same range as in the anion of *trans*-$[Bu_4N][Ru(RCN)_2Cl_4]$ (2.353 Å) [13c,18] (R = Me, Ph) but shorter than that in $[Ru(CH_3CN)_4Cl_2]$ [15a] (2.410 Å), whereas the average Ru–N distance in **2** (2.020 Å) is comparable with that in $[Ru(CH_3CN)_4Cl_2]$ [15a] (2.025 Å). The C–N distance in the coordinated CH_3CN molecules (1.138 Å) is formally shorter than the C–N distance in the non coordinated CH_3CN (1.19 Å). The coordinated CH_3CN is bent. The astonishingly small angle N(3)–C(31)–C(32) (158(5)°) is yet unexplained. **3** has a meridional–octahedral geometry. The distances Ru–Cl(1), Ru–Cl(3), Ru–Cl(4) and Ru–Cl(6) are longer than Ru–Cl(2) and Ru–Cl(5) as well as Ru–N(3) and Ru–N(6) in relation to Ru–N(1), Ru–(2), Ru–N(4) and Ru–N(5) because of the bigger *trans* influence of Cl related to CH_3CN and in accordance with corresponding results for acetonitrile-*mer*-trichloro [1-methyl-3-(2-pyridyl)-1,2,4-triazole-N(4), N(1′)]ruthenium [19] and for $\{[Ru(C_6H_5CN)_3Cl_3]_{0.5}[C_6H_5CN]\}$ [13c].

2.3. Voltammetric analysis of *3*

The stability of **3** through the transition $Ru(CH_3CN)_3Cl_3]/[Ru(CH_3CN)_3Cl_3]^{+1}$ was mentioned already by Duff and Heath [13a] and as shown below, it is stable as a redox mediator. Both its CV steps (Fig. 4) are reversible single-ET steps over sweep rates of 50–1000 mV s^{-1}. At 1000 mV s^{-1} in absence of *i*R correction, $\Delta E_p = 80 \pm 3$ mV, $\Delta E_{1/2} = 60 \pm 3$ mV, $i^c/i^a = 0.9 \pm 0.05$. The plot of i_p versus $v^{1/2}$ at 1840 mV is linear over $v = 50$–1000 mV s^{-1}. At 133 mV the plot of i_p versus $v^{1/2}$ shows a break in linearity above 100 mV s^{-1}, suggesting slow ET relative to the rate of mass transport under fast scan (Fig. 6) [20]. Voltammograms of **3** with ferrocene as standard (500 mV) also establish the redox transitions of **3** as single ET steps. The ratio of diffusion coefficients of **3** to ferrocene was found to be 0.66 and was taken into account.

Because of the substantial differences in reference electrodes and experimental conditions like solvents and temperature it is difficult to make comparisons with the previous data even with consideration of ferrocene as standard [13a]. $E_{1/2}^c$ at 290 mV reported for $Ru(CH_3CN)_3Cl_3$ [13a] differs from our results of 133 mV for 3. The second CV given for $Ru(CH_3CN)_3Cl_3$ at 1890 mV ($E_{1/2}^c$) [13a], is close to our value of 1840 mV (E_p^a) of **3**. The reported value of 1450 mV for $Ru(CH_3CN)_2Cl_4$, is also comparable to our value of 1350 mV for **2** but still different. The assignments in Table 1 are concluded from the present measurements (as in Figs. 1, 3 and 4).

As mentioned above, ligand exchanges in the series $Ru(CH_3CN)_nCl_{6-n}$ can be electrically induced [13]. It is

Table 1
Redox states proposed for the isolated ruthenium–acetonitrile compounds [a]

	Ru(II/III) (mV)	Ru(III/IV) (mV)	Ru(IV/V) (mV)
$Ru(CH_3CN)_4Cl_2$ (**1**)	753	NA	
$Ru(CH_3CN)_3Cl_3$ (**3**)	133	1840	
$Ru(CH_3CN)_2Cl_4$ (**2**)		a	1350

[a] Values are of E_p^{oxid} observed within the window of −1.5 to +2.3 V in CH_3CN, reference electrode Ag | AgCl. NA, not available. a Reduction is observed at −570 mV. Assignment uncertain.

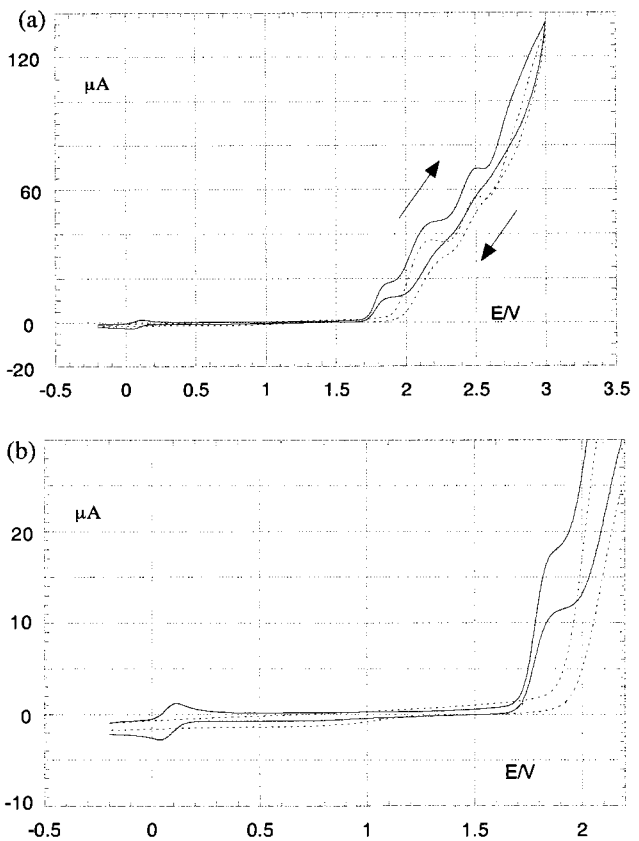

Fig. 7. (a) Catalytic current of $Ru(CH_3CN)_3Cl_3$ (**3**), shown at 1840 mV when tetralin 5×10^{-3} M, is scanned in the presence of $Ru(CH_3CN)_3Cl_3$ (**3**) 10^{-3} M, solid line. Background: 5×10^{-3} M tetralin only. CV at 50 mV s^{-1} in 25 ml CH_3CN, 0.1 M TBAP. Scan from zero current towards positive potential (oxidation current positive) upper curve. Return: (lower curve). (b) Enlarged detail.

therefore important to note that the reversibility and stability of the structure of **3** over many redox cycles implies that the ET steps observed as in Fig. 4, involve no change in the structure of this complex. The most reasonable redox transitions are suggested in Eq. (2):

$$[Ru(CH_3CN)_3Cl_3]^- \underset{+e}{\overset{-e}{\leftrightarrows}} [Ru(CH_3CN)_3Cl_3] \underset{+e}{\overset{-e}{\leftrightarrows}} [Ru(CH_3CN)_3Cl_3]^+ \quad (2)$$

The reported stability of the anion $[Ru(C_6H_5CN)_2Cl_4]^-$ [17] and the reversibility of the step: $Ru(CH_3CN)_3Cl_3]/[Ru(CH_3CN)_3Cl_3]^{+1}$ [13a], support such conclusions. The structures, stability and ET features of **1**, **2** and particularly **3** are therefore established.

2.4. Catalysis

So far, catalysis was observed with compound **3**. Compounds **1** and **2** do not show interactions in any of the following cases. Compound **3** acts as a reversible ET mediator for the oxidation of cyclohexene, 1-methylcyclohexene, 4-methylcyclohexene, tetralin and 1-hydroxy-tetralin, as seen by CV. All these compounds oxidize above 1900 mV and in their presence the CV trace of **3** at 1840 mV is transformed into a catalytic curve. At the same time in these cases, the CV profile at 133 mV remains unchanged through repeated catalytic cycles. This is an extra indication that the coordination sphere of **3** survives the catalytic cycle. It also serves as a useful internal standard for the concentration of the catalyst during CV and in the course of preparative electrolysis (Fig. 7). A similar situation, in which an ET reduction catalyst carried an internal marker, has been observed by Lund and Simonet [21]. In other cases, internal standards were attached to heterogeneous catalysts on modified electrodes [22].

Tetralin was selected for a detailed study of the catalysis by preparative electrolysis. The CV of tetralin alone and in presence of **3** is shown in Fig. 7. When a small amount of **3** is added, its relative concentration is clearly seen at 133 mV. The catalytic current appears at 1850 mV and shows a tenfold increase relative to the 133 mV marker. The catalytic current appears at a value where tetralin is not electroactive. It is characteristic of an EC reaction [23] with the expected Nernstian shift of the reverse (reduction) potential, the absence of the reverse (reduction) current, the limiting value of i_p above 100 mV s^{-1} and decrease of $[i_p/(v)1/2]$ versus v. The current intensities observed at potentials above 2.0 V in the direct oxidation of tetralin, also increase in presence of **3**.

CPE of tetralin in acetonitrile with $LiClO_4$ or TBAP as electrolyte, was carried out at a potential of 1400 mV versus Ag | $AgBF_4$. This is 200 mV below the over-potential for direct oxidation of tetralin [24]. A sample run with $LiClO_4$ as electrolyte, starting with 45×10^{-5} mol tetralin and 2.5×10^{-5} mol **3**, gave 29% conversion in 4 h. A charge equivalent of 26.3×10^{-5} e mol^{-1} was passed. Accordingly **3** has made over 10.5 cycles namely, a turnover rate of 1.25 h^{-1} where turnover rate = mol tetralin oxidized mol catalyst^{-1} h^{-1}. Current efficiency for consumption of tetralin if taken as two 1 e steps is > 98%. The same run after 5.5 h reached 35.5% conversion. A charge equivalent of 32.9×10^{-5} e mol^{-1} was passed. Here **3** has made over

13 cycles, a turnover rate of 1.145 h^{-1}. Under the same conditions with TBAP as electrolyte the initial reaction rate is 6×10^{-6} M min^{-1}, about 3.5 times slower than with $LiClO_4$, current yields are 65–67%, and the turnover rate of the catalyst is 0.93–0.95 h^{-1}, 20% lower with TBAP.

No reaction at all takes place, nor any current produced at this potential without catalyst. The direct, uncatalyzed reaction at 1900 mV (2300 mV vs. Ag | AgCl), shows a current efficiency of 64% for two 1 e steps. Thus, the catalytic current observed in voltammetry fully accounts for the oxidation of tetralin.

An undivided cell has been used in this work and in the course of the reaction, **3** is slowly reduced to **1**, obviously a reduction by H_2 on the cathode. With the progress of reaction, intensity of the reversible CV for **3** at 133 mV decreases and the reversible CV for **1** at 753 mV appears and increases. Cell division prevents loss of catalyst and there is practically no reduction of **3** when it is electrolyzed in the anodic compartment of a cell, divided by fritted glass.

Reactions were followed by HPLC and GC–MS. Scheme 1 shows that the products obtained by catalyzed CPE are those expected from reactions of a radical–cation or of the derived cation, with any of the available nucleophiles [25]. A sample of products after removal of electrolyte; with unavoidable loss of material, shows: tetralin (43.5%), 1,2-dihydronaphthalene (4.4%) 1-tetralol (10.4%) 1-tetralone (27.8%) acetamidotetralin (13.8%), chlorotetralin (0.1%) (reaction 3 in Section 4.3.4, average of two analyses). Dihydronaphthalene from deprotonation and oxidation of the radical–cation; an ECEC process, 1-tetralol and 1-tetralone from reaction with water (0.03% in acetonitrile). The general pattern in all runs is: 1-tetralone > 1-tetralol ≫ dihydronaphthalene. Particular yields depend on charge and reaction time. 1,2-Dihydronaphthalene forms early in the reaction, always in small amounts and reacts further, by oxidation to tetralone or presumably by polymerization. CV of 1,2-dihydronaphthalene shows $E_p^{oxid} = 1680$ mV (160 mV lower than the 1840 mV of **3**), and no interaction with **3**. It therefore oxidizes directly. Tetralol, with the same E_p^{oxid} as tetralin responds to **3** in the same way as tetralin, with a catalytic current and is an intermediate in formation of tetralone. 1-tetralone with $E_p^{oxid} = 2.6$ V shows no interaction with **3** and at 1840 mV accumulates as a final product. Hence the reasons for selectivity for tetralone. Acetamidotetralin reflects the reaction of the radical–cation or cation with the solvent, particularly in the direct, uncatalyzed reaction under high potentials. The reduced potential of the indirect electrolysis is an effec-

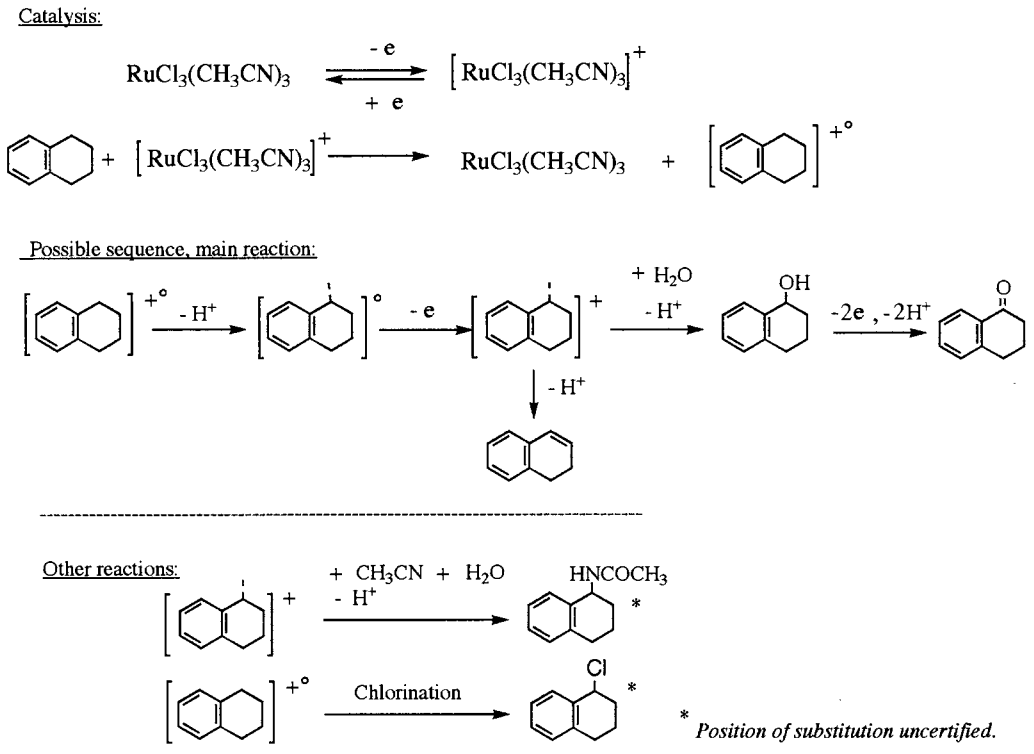

The issue of deprotonation of radical cations is discussed in detail in
A. Anne, S. Fraoua, V. Grass, J. Moiroux and J.M. Saveant, *J.Amer.Chem.Soc.* 120 (1998) 2951.

Scheme 1.

tive means to circumvent this side reaction. Acetamidation is itself an interesting reaction. Chlorotetralin has been detected only in trace amounts and only in one run out of ten, an exception that possibly indicates a minor route for the disintegration of **3**. Mere presence of chloride anions is not enough. No chlorination is observed when tetralin is electrolyzed at 1840 mV (Ag | AgCl), with tetraethylammonium chloride 0.1 M as electrolyte.

With $LiClO_4$ as an electrolyte, current yields are high and product separation is easy. When TBAP is used as electrolyte instead, current efficiency is in the range of 60–66% for a 2 e step. Yields in this case are lower because the work-up and separation of electrolyte are more tedious.

In terms laid down by Andrieux et al. [26], **3** is a typical ET catalyst, and acts specifically on the initial step of oxidation to create the radical cation. Therefore the obvious advantage of electrolysis aided by **3** is mainly the reduction in the required oxidation overpotential and an accelerated charge transfer. This ultimately affects selectivity by favoring products with lower oxidation potentials and prevents follow-up oxidation. There is also some selectivity in regard with **3**. Several aromatic compounds like naphthalene and methyl naphthalene, which oxidize at 1.65 V and are affected by $RuCl_3$ [8], or like dihydronaphthalene mentioned above, do not interact with **3**. They oxidize at potentials lower than 1.850 V. Electron transfer is after all not only a question of potential [1] and selectivity also depends on factors such as reorganization energy. For example, 4-chlorotoluene, which has been oxidized by electrogenerated Ru(IV) compounds [27,28] shows a current increase above 1840 mV in the presence of **3** but not a catalytic wave and no catalytic effect was verified in that case by controlled-potential electrolysis.

3. Conclusions

Three complexes have been isolated from the solution of $RuCl_3 \cdot 3H_2O$ in acetonitrile. Their structures and redox chemistry were studied. Compound **3** is found to be a singular redox mediator, capable of converting substances that have an intrinsic higher oxidation potential. The oxidation of tetralin was examined in some detail. It is also noted that **3** reacts only with specific compounds as mentioned above, depending possibly on their structure as well as their redox potential. It should be possible to tune the catalytic activity to other cases by modifications of ligands in RuL_3Cl_3 and explore further possibilities in the RuL_nX_{6-n} series.

The advantage of electrochemical methods over pure chemical methods is in safety and mild conditions, in easy adaptation to flow methods, and in linear scale-up. The mediated method has a further advantage over direct electrolysis in providing appreciable current densities at low potentials where the direct oxidation is inactive. Electrochemical oxidation of hydrocarbons has been widely reported [2–5] with use of additives such as RuO_4, MnO_4, cerium salts and others in situ or in separate cells. All these additives are seldom catalytic, are required in large amounts and are harmful for the environment. $KMnO_4$ was used in a specific example to convert tetralin to tetralone [29] electrochemically in a membrane divided cell with a phase transfer catalyst. The indirect electrolysis with **3**, is a simpler procedure. The homogeneous oxidation of tetralin which is based on hydrogen-transfer to a sacrificial aldehyde, tends to over-run the tetralone stage when catalyzed by metal complexes to yield also 1,4-di-keto-2,3-dihydronaphthalene and other products [30]. The catalyzed anodic process does not over-run the stage of tetralone.

4. Experimental

4.1. General

NMR measurements were taken on a Bruker spectrometer 300 MHz. IR spectra were obtained with a Nicolet, Impact 400 spectrophotometer. Diffraction analysis was performed with an Enraf–Nonius CAD4 automatic diffractometer. Electrospray ionization (EIS) mass spectrometry of compound **3** was performed on a Finingan LCQ (ESI–Iontrap–MS). GC–MS was performed with a model HP 5989A on 5% silicon HPI capillary column. HPLC was performed on a Tracor model 970 A on a C18 reversed phase column and voltammetric measurements were carried out with a PAR Versastat model 253.

Solvent was degassed and all procedures other than hydrogenation were carried out under Ar. Dry acetonitrile (Aldrich or Mallinckrodt) was HPLC quality, containing 0.03% water.

4.2. Hydrogenation of $RuCl_3 \cdot 3H_2O$

A solution of $RuCl_3 \cdot 3H_2O$ (Johnson Matthey, 1.5 g) in acetonitrile (20 ml), with 0.010–0.015 g of 5%Pt/C (Aldrich catalogue 33,015-9) was stirred in dry acetonitrile by a slow stream of hydrogen (ca. 20 bubbles min^{-1}) at 15–20°C. An orange precipitate collected in the course of several hours (7–15). At a suitable stage (see below), the precipitate was filtered off and dried under a stream of Ar. The amount of filtered precipitate was about 1.2–1.5 g. If the hydrogenation was prolonged (10–24 h) or the precipitate treated further with hydrogen, the product turned yellow–green to yield mostly **1**. The reaction is not homogeneous and the time required depends very much on the catalyst.

CV analysis of solution and precipitate was taken at 1 h intervals. The CV trace for $RuCl_3 \cdot 3H_2O$ was very complex and obscure. After several hours of hydrogenation, potential scans of the solution and precipitate showed distinct CV waves indicating a mixture of several compounds. Mixtures of **1**, **2** and **3**, can be recognized within 7–15 h (Fig. 1). Some unidentified products were also present. The suitable stage for separating the precipitate is when concentration of a compound (**1**, **2** or **3**), is judged optimal from CV. Compound **2** was obtained from a short hydrogenation time (6 h) by collecting the precipitate and crystallization from CH_3OH. From 1 g of powder consisting of **2** and **3**, crystals of **2** (about 50 mg) were isolated after several days in a saturated solution of CH_3CN–$CHCl_3$. In a typical run, the crude precipitate shows a composition as in Fig. 1 where **3** and **2** appear in proportions of 3:1. From 1.5 g of $RuCl_3 \cdot 3H_2O$, 1.5 g precipitate was obtained after 14 h hydrogenation with a ratio of 3:1 for **3** and **2**. That gives a rough estimate of yields as 40% **3** and 13% **2**. From this, **3** was purified by column chromatography on silica gel, with CH_3CN–CH_2Cl_2 (1:1) as eluant, to yield 1 g of a brick-red colored complex, m.p. (dec) 180°C. CV as in Fig. 4. IR at 2327 cm^{-1} (C≡N stretching). (CH_3CN shows 2295 and 2253 cm^{-1}.) Anal. Calc. for dry powder: C, 21.8; H, 2.74. Found: C, 21.9, 22.1; H, 2.92, 2.92%. Crystal growth from the powder with a small amount of CH_3CN–CH_2Cl_2 (1:1) at 20°C ± 5, is very slow and takes several weeks. The crystals and powder have CV as in Fig. 4. Compounds **2** and **3** also separate by TLC on alumina by solvents like $CHCl_3$, CH_2Cl_2 and mixed eluants.

Prolonged hydrogenation or hydrogenation of **3** yields **1** as a yellow–green precipitate.

4.2.1. Mass spectra of 3

MS by ESI of **3** shows $[Ru_2(CH_3CN)_6Cl_6Na]$ aggregates. Highest intensity clusters: $[Ru_2(CH_3CN)_6Cl_6Na]^+$ m/z average 684.20335, with m/z peaks ranging from 673.7 to 694.9 around highest peak at 683.2, $[Ru_2(CH_3CN)_4Cl_6Na]^+$ m/z around highest peak at 602.3, $[Ru(CH_3CN)_3Cl_3Na]^+$ m/z around highest peak at 354.7, all closely fit with simulation of the expected isotope clusters.

Sodium adducts: in the course of spraying, uncharged compounds may become ionized by protons, or if not basic enough, by alkali ions, ubiquitous sodium ions in this case.

4.3. Electrochemistry

Voltammetry was conducted in a three electrode cell. Working electrodes were 2 mm^2 tips of a 1 mm Pt wire, counter electrode a 1 cm^2 piece of Pt or steel, in acetonitrile with 0.1 M TBAP. Reference electrode for voltammetry was $Ag \mid AgCl \mid KCl\ 3\ M \mid$. Voltammetry was also performed with $Ag \mid AgBF_4$ (0.1 M) as reference. For compounds **1**, **2** and **3** as well as the mixtures, scanning was performed from various points of the potential scale. The same curve is retained when scans are started at different positions within the range shown, or run against a different reference ($Ag \mid AgBF_4$). For example, **3** is seen in Fig. 1 and in Fig. 4 from different directions, as is **2** in Fig. 1 and in Figs. 3a and b.

Voltammograms of **2**; voltammograms of **2** as shown in Fig. 3 are of crystals. Scanning from positive or negative potential, as well as separate scans for oxidation and reduction gives the same two curves, at 1330 mV (reversible) and at −600 mV (irreversible reduction).

Voltammograms of **3**; When the two CV positions (Fig. 4) are analyzed individually, at scan rates between 50 and 1000 mV s^{-1}, $i^c/i^a = 0.95$ at 133 mV and $i^c/i^a = 0.88 \pm 0.3$ at 1850 mV. The values $\Delta E_{1/2} = 58 \pm 3$ mV, $\Delta E_p = 75 \pm 5$ mV were the same for both CV curves. Such parameters are expected for reversible single-electron steps [20]. Voltammograms of ferrocene (508 mV) together with **3** in predetermined quantities, show that the redox processes of **3** are single electron steps as determined by the values of ΔE and i_p. Ferrocene can only be matched against the CV at 133 mV, as at 1820 mV unexplained catalytic currents are observed. The ratio of diffusion coefficients of ferrocene and of **3**, was found by chronoamperometry. Potential steps were applied at 800 mV ($Ag \mid AgCl$) and diffusion coefficients D (D_3 for **3**; D_f for ferrocene), calculated from the slope of i versus $1/t^{1/2}$. For ferrocene $n = 1$. Assuming $n = 1$ for **3**, $(D_3)/(D_f) = 0.66 \pm 0.09$. The ratios of peak currents in CV, of same solutions, were found as $(i_3)/(i_f) = 0.7 \pm 0.07$ for the first redox at 133 mV.

Catalytic currents; voltammetry of solutions of **3** ($\sim 10^{-4}$ M) shows catalytic currents at 1840 mV with cyclohexene, methylcyclohexene, ferrocene, tetralin and 1-tetralol. The products of tetralin oxidation, 1-tetralone $E_p^{oxid} = 2.6$ V and 1,2-dihydronaphthalene $E_p^{oxid} = 1680$ mV, do not show interaction with **3**.

Controlled-potential electrolysis; controlled-potential electrolysis (CPE) of tetralin in undivided three electrode cells, in 50 ml acetonitrile solutions, was run on 1 cm^2 Pt working electrode at the potential of 1400 mV unless otherwise stated, versus $Ag \mid AgBF_4$ (0.1 M) with fritted glass separation as reference electrode. Electrolyte in CPE was 0.1 M $LiClO_4$ or 0.1 M TBAP. Sample runs in the presence or absence of **3** are given below.

4.3.1. Non-catalyzed CPE at low potential — reaction 1

At 1.4 V. [**3**] = 0, $LiClO_4$ 0.1 M, quantity of tetralin 45×10^{-5} mol, potential set at 1.4 V ($Ag \mid AgBF_4$).

Only negligible current is observed, no loss of tetralin, nor any oxidation was detected after 3 h.

4.3.2. Direct CPE at high potential — reaction 2 (a) non-catalyzed

Reaction was run at 1.9 V (see Fig. 7). $LiClO_4$ was 0.1 M, [**3**] = 0, tetralin quantity was 44×10^{-5} mol. Reaction time was 4 h, charge passed 22×10^{-5} F, tetralin converted was 7×10^{-5} mol (15.9%), current efficiency for two 1 e steps is therefore $\sim 64\%$. Initial rate is $d[\text{Tetralin}]/dt = 5 \times 10^{-7}$ mol min^{-1}, calculated as an average over the first 30 min.

4.3.3. Direct CPE at high potential — reaction 2 (b) catalyzed

CPE, was carried out direct, at 1.9 V in the presence of **3**. Reaction 8: initial quantities were: **3** 2.5×10^{-5} mol, tetralin 45×10^{-5} mol. Reaction time was 4 h, charge passed 41.4×10^{-5} F, tetralin converted 17×10^{-5} mol (37.7%), current efficiency 82%. Initial rate over first 30 min. $d[\text{Tetralin}]/dt = 3.10^{-5}$ mol min^{-1}.

4.3.4. Indirect CPE-catalyzed, low potential — reaction 3

At 1.4 V (see Fig. 7). $LiClO_4$ 0.1 M, Quantities in the sample: **3** $= 2.5 \times 10^{-5}$ mol, tetralin 45×10^{-5} mol (initial). Reaction time 4 h, charge passed 26.3×10^{-5} F, tetralin converted 13×10^{-5} mol (29%) (by HPLC), current efficiency $\sim 98\%$. Reaction time 5.3 h: 29×10^{-5} mol (final), (35.5% converted), hence 16×10^{-5} mol consumed, charge passed 31.7 C (32.86×10^{-5} F). Current efficiency for two 1 e steps is 98%. Initial rate (first 30 min), $d[\text{Tetralin}]/dt = 1.5 \times 10^{-6}$ mol min^{-1}. Reaction under the same conditions with 0.1 M TBAP instead of $LiClO_4$ shows 21.6% conversion after 4 h, 28 C (29×10^{-5} F), a current efficiency of 65%. The composition of a sample of isolated products mixture after 5.3 h, is given in the results section.

4.3.5. Effect of water

Reaction under the same conditions as reaction 3, with 0.1 M TBAP and increasing concentrations of water to 0.1 M (untreated acetonitrile has 0.03%, 0.017 M water), shows 16.5% conversion after 4 h, 23 C (24×10^{-5} F), a current efficiency of 61%.

4.4. Products from CPE

Tetralone is the main product, accompanied by 5–20% tetralol depending on run and reaction time. Tetralol is an intermediate and oxidizes to tetralone. Dihydronaphthalene and naphthalene are in small amounts in the low potential runs. Tetralin, tetralol, tetralone and 1,2-dihydronaphthalene were identified by HPLC and GC–MS and compared with authentic samples (Aldrich). Tetralin conversion and tetralone formation was followed in the course of CPE on HPLC based on calibration graphs. Between 9 and 10 samples were taken at predetermined times in each run. Tetralone gives a strong HPLC signal as compared to tetralin, tetralol and other products, due to the high response factor of the UV detector.

GC–MS from reactions 2–3 shows m/z (%): tetralin = 132(46), 117(12), 115(12), 104(100), 91(4); 1,2-dihydronaphthalene 131(54), 130(100), 129(35), 119(27), 115(19), 91(4); 1-tetralol 148(42), 147(38), 131(19), 130(100), 129(38), 120(92), 119(54), 115(23), 105(42), 104(8), 91(58); 1-tetralone 146(69), 131(15), 118(100), 115(12), 104(4), 90(65); 1-acetamidotetralin (identified by GC–MS only): 189(7), 146(13), 131(16), 130(100), 129(25), 119(11), 118(4), 117(2), 115(11), 91(7) (from reaction 3, trace amount).

Acetamidotetralin m/z 189 was found in uncatalyzed direct reactions at high potential. Chlorotetralin was detected in trace amounts in one catalyzed run only (out of ten), and identified by GC–MS only. Tetralin itself contains trace impurities $m/z = 130$ $m/z = 128$ presumably 2,3-dihydronaphthalene and naphthalene.

Electrolysis of **3**; A 'H-shaped' cell with a fritted glass separator was used with Pt electrodes as above with 90 ml acetonitrile solutions of TBAP 0.1 M in each compartment. Compound **3**, 2.5×10^{-5} mol (2.8×10^{-4} M) was added to the anode compartment and electrolyzed at 1.4 V ($Ag \mid AgBF_4$) for 3 h, under a steady current of 130 μA. Altogether, 1.4 C was passed. The solution was scanned by CV at predetermined times. There was no change in **3**. The cell was reversed and with **3** in the catholyte its concentration dropped rapidly with build up of the reversible CV signal of **1**. Over 2 h, the current dropped from 250 to 60 μA, during which, 0.6 C were passed.

4.5. X-ray structure determination of **2** and **3**

Crystal data and other details of the structural determination are collected in Table 2 Data collections were carried out with an Enraf–Nonius CAD4 automatic diffractometer ($\omega - 2\theta$ scan, $\lambda = 0.71096$ Å, variable scan time 45 s), controlled by a PC fitted with a low-temperature equipment. The cell parameters were obtained from a least-squares treatment of the SET4 setting angles of 25 reflections in the range of $12.7° < 2\theta < 24.2°$ for **2** and $10.16° < 2\theta < 26.4°$ for **3**. Reflections were scanned with variable scan time, depending on intensities, with 2/3 of the time used for scanning the peak and 1/6 measuring each the left and the right background. The intensities of three check reflections monitored every 2 h showed only statistical fluctuations during the data collection. The orientation of the crystal was checked every 200 intensity measurements by scanning three strong reflections well distributed in reciprocal space. A new orientation matrix would have

Table 2
Crystal data and structure refinement for **2** and **3**

	2	**3**
Empirical formula	$C_6H_{11}Cl_4N_3ORu$	$C_{16}H_{24}Cl_6N_8Ru_2$
Formula weight (g mol^{-1})	384.05	743.27
Temperature (K)	163(2)	163(2)
Crystal system	Monoclinic	Triclinic
Space group	$P2_1$	$P\bar{1}$
Unit cell dimensions		
a (Å)	8.238(2)	8.6294(10)
b (Å)	7.700(7)	12.146(6)
c (Å)	11.842(3)	14.808(5)
α (°)		82.92(4)
β (°)	106.86(2)	87.31(2)
γ (°)		74.92(2)
Volume (m^3)	$718.9(7)\times10^{-30}$	$1487.0(9)\times10^{-30}$
Z	2	2
D_{calc} (g cm^{-3})	1.774	1.660
Absorption coefficient (mm^{-1})	1.814	1.574
$F(000)$	376	732
Crystal size (mm^3)	$0.18\times0.18\times0.27$	$0.18\times0.15\times0.15$
Aperture (mm)	2.3	2.3
Scan angle (°)	$(0.83+0.35\tan\theta)$	$(1.1+0.35\tan\theta)$
θ Range for data collection (°)	$3.6<2\theta<47.86$	$2.78<2\theta<45.90$
Index ranges	$0\le h\le9$, $0\le k\le8$, $-13\le l\le12$	$-2\le h\le9$, $-12\le k\le13$, $-16\le l\le16$
Reflections collected	1312	4535
Independent reflections	1222 [$R_{int}=0.0370$]	4118 [$R_{int}=0.0459$]
Refinement method	Full-matrix least-squares on F^2	Full-matrix least-squares on F^2
Data/restraints/parameters	1214/0/124	4104/0/297
Goodness-of-fit on F^2 [c]	1.050	1.011
Final R indices $[I>2\sigma(I)]$ [a,b]	$R_1=0.0382$, $wR_2=0.0940$	$R_1=0.0426$, $wR_2=0.0861$
R indices (all data)	$R_1=0.0652$, $wR_2=0.1141$	$R_1=0.0927$, $wR_2=0.1092$
Absolute structure parameter	−0.1(2)	
Largest difference peak and hole (e Å^{-3})	1.198 and −0.971	0.520 and −0.499

[a] $R_1=(F_o-F_c)/F_o)$.
[b] $wR_2=[w(F_o-F_c)^2/wF_o^2]^{1/2}$.
[c] Goodness-of-fit $=[w(F_o-F_c)^2/(n-p)]^{1/2}$.

automatically been calculated from a list of 25 re-entered reflections, if the angular change was larger than 0.1%. The raw data were corrected for Lorentz, polarization and absorption effects [31]. The positions of the heavy atoms were determined with direct methods (SHELXS-86) [32]. Structure solution and refinement were carried out with the SHELXS-86 [31] and SHELXL-93 [33] software, respectively. The non-hydrogen atoms were refined with anisotropic temperature factors. The hydrogen atoms were calculated in idealized positions (C–H = 0.96 Å, $U_{iso}=0.08$ Å^2). Scattering factors were taken from Ref. [34] The non-hydrogen atoms of the solvent molecules were refined with isotropic temperature factors. Data reduction was performed using PC-software [30]. All other calculations were done with SHELXL-93 [32]. Molecular plots were obtained with the program ZORTEP [35], thermal ellipsoids were scaled to 50% probability level.

5. Supplementary material

Crystallographic data for the structural analysis have been deposited with the Cambridge Crystallographic Data Centre, CCDC no. 131449 for compound **2** and no. 131450 for compound **3**. Copies of this information may be obtained free of charge from The Director, CCDC, 12 Union Road, Cambridge, CB2 1EZ, UK (Fax: +44-1223-336033; e-mail: deposit@ccdc.cam.ac.uk or www: http://www.ccdc.cam.ac.uk).

Acknowledgements

This work has been supported by a research grant from the German–Israeli Fund (GIF). Diffraction analysis was supported by the Deutsche Forschungsgemeinschaft (Graduiertenkolleg Synthetische, mechanistische und reaktionstechnische Aspekte von Metallkatalysatoren) and the Technische Universität Berlin (Partnerschaft TUB-HUJ). The authors also thank Dr H. Luftmann from the Organisch-Chemisches Institut der Universität Münster, Germany for the ESI MS of **3**, and J. Katzir from the Technion Israel and Y. Norbert of HUJ for GC–MS analysis.

References

[1] D. Astruc, Electron Transfer and Radical Processes in Transition-Metal Chemistry, VCH, New York, 1995.
[2] (a) E. Steckhan, Top. Curr. Chem. 1 (1987) 142. (b) J. Simonet, in: H. Lund, M.M. Baizer (Eds.), Organic Electrochemistry, Marcel Dekker, New York, 1991, p. 1217. (c) M.M. Baizer, in: H. Lund, M.M. Baizer (Eds.), Organic Electrochemistry, Marcel Dekker, New York, 1991, p. 1265.
[3] C. Moinet, J. Phys. IV 4 (recent developments in electrochemistry) (1994) 175.
[4] (a) C. Amatore, M. Bayachou, F. Boutejengout, J.N. Verpeaux, Bull. Soc. Chim. Fr. 130 (1993) 371. (b) T. Inokuchi, T. Sugimoto, M. Kusumoto, S. Torii, Bull. Chem. Soc. Jpn. 65 (1992) 3200. (c) T. Inokuchi, P. Liu, S. Torii, Chem Lett. 8 (1994) 1411. (d) D. Pletcher, in: R.D. Little, N.L. Weinberg (Eds.), Electroorganic Synthesis (M.M. Baizer memorial symposium 1990), Marcel Dekker, New York, 1991, p. 255. (e) M.L. Tsai, T.C. Chou, J. Chin. Inst. Chem. Eng. 27 (1996) 411. (f) J. Heyer, S. Dapperheld, E. Steckhan, Chem Ber. 121 (1988) 1617. (g) D. Lexa, J.-M. Savéant, H.J. Schäfer, K.-B. Su, B. Vering, D.L. Wang, J. Am. Chem. Soc. 112 (1990) 6162. (h) T. Bechtold, E. Burtscher, A. Amann, O. Bobleter, Angew. Chem. Int. Ed. Engl.

31 (1992) 1068. (i) S.I. Kulakovskaya, V.M. Berdnikov, A.A. Vasilenko, A.Ya. Tikhonov, L.B. Volodarskii, Russ. J. Electrochem. (Elektrokhimiya) 32 (1996) 784. J.D. Pletcher, H. Thompson, J. Electroanal. Chem. 464 (1999) 168.

[5] (a) O.N. Efimov, V.V. Strelets, Coord. Chem. Rev. 99 (1990) 15. (b) T. Inokuchi, M. Kusumoto, S. Torii, in: R.D. Little, N.L. Weinberg (Eds.), Electroorganic Synthesis (M.M. Baizer memorial symposium 1990), Marcel Dekker, New York, 1991, p. 233. (c) T. Takiguchi, T. Nonaka, Chem. Lett. 6 (1987) 1217. (d) S. Kwee, Bioelectrochem. Bioenerg. 16 (1986) 99. (e) M. Navarro, W.F. De Giovani, J.R. Romero, Tetrahedron 47 (1991) 851.

[6] B.R. James, Inorg. Chim. Acta Rev. 4 (1970) 73.

[7] M.M. Taqui Khan, A. Prakash Rao, S.H. Mehta, J. Mol. Cat. 78 (1993) 263.

[8] (a) S. Chocron, M. Michman, J. Mol. Cat. 66 (1991) 85. (b) M. Michman, M. Oron, Electrochim. Acta 39 (1994) 2781. (c) M. Michman, J. Mol. Cat. A 107 (1996) 393.

[9] M. Oron, Ph.D. Thesis, The Hebrew University of Jerusalem, 1999.

[10] E.A. Seddon, K.R. Seddon, The Chemistry of Ruthenium, Elsevier, Amsterdam, 1984, p. 159.

[11] N.N. Greenwood, A. Earnshaw, The Chemistry of the Elements, Pergamon, Exeter, 1984, p. 1259.

[12] J. Dehand, J. Rosé, J. Chem. Res. S (1979) 155.

[13] (a) C.M. Duff, G.A. Heath, Inorg. Chem. 30 (1991) 2528. (b) C.M. Duff, G.A. Heath, J. Chem. Soc. Dalton Trans. (1991) 2401. (c) C.M. Duff, G.A. Heath, A.C. Willis, Acta Crystallogr. Sect. C 46 (1990) 2320.

[14] N.N. Greenwood, A. Earnshaw, The Chemistry of the Elements, Pergamon, Exeter, 1984, p. 1069.

[15] (a) D.E. Fogg, S.J. Rettig, B.R. James, Can. J. Chem. 73 (1995) 1084. (b) W.E. Newton, J.E. Searles, Inorg. Chim. Acta (1973) 7349.

[16] J.D. Gilbert, D. Rose, G. Wilkinson, J. Chem. Soc. A (1970) 2765.

[17] A sample of $Ru(CH_3CN)_4Cl_2$ was kindly provided by B.R. James of UBC, Vancouver.

[18] D. Ooyama, N. Nagao, F. Scott Howell, M. Mukaida, H. Nagao, K. Tanaka, Bull. Chem. Soc. Jpn. 68 (1995) 2897.

[19] R. Hage, R. Prins, A.G. de Graaff, J.F. Haasnoot, J. Reedjik, J.G. Vos, Acta Crystallogr. Sect. C 44 (1988) 56.

[20] R. Greef, R. Peat, L.M. Peter, D. Pletcher, J. Robinson, Instrumental Methods in Electrochemistry, Southampton Electrochemistry Group, Ellis Horwood, Chichester, 1985.

[21] H. Lund, J. Simonet, J. Electroanal. Chem. 65 (1975) 205.

[22] I. Rubinstein, Anal. Chem. 56 (1984) 1135.

[23] A.J. Bard, L.R. Faulkner, Electrochemical Methods, Fundamentals and Applications, Wiley, Chichester, 1980, p. 433, see also Ref. [19] p. 196.

[24] The $Ag \mid AgCl$ reference is replaced by $Ag \mid AgBF_4$ which is stable in the course of prolonged CPE in acetonitrile. All potential readings are -400 mV down from $Ag \mid AgCl$, hence 1400 mV vs. $Ag \mid AgBF_4$ is equivalent to 1800 mV in the CV (Fig. 7).

[25] L. Eberson, J.H.P. Utley, O. Hammerich, in: H. Lund, M.M. Baizer (Eds.), Organic Electrochemistry, Marcel Dekker, New York, 1991, p. 505.

[26] C.P. Andrieux, J.M. Dumas-Bouchiat, J.M. Savéant, J. Electroanal. Chem. 87 (1978) 39 and 55.

[27] M.S. Thompson, W.F. De Giovani, B.A. Moyer, T.J. Meyer, J. Org. Chem. 49 (1984) 4972.

[28] B.A. Moyer, M.S. Thompson, T.J. Meyer, J. Am. Chem. Soc. 102 (1980) 2310.

[29] P.L. Matlock, R.M. Sandner, US 4,277,318, 1980 (to Union Carbide Corp.) Chem. Abstr. 95 (1981) 88 237c.

[30] M.M. Dell'Anna, P. Mastrorilli, C.F. Nobile, J. Mol. Cat. A 130 (1998) 65.

[31] R. Fröhlich, XCAD4, Program for Data Reduction, University of Münster, 1994.

[32] G.M. Sheldrick, SHELX-86, Program for Crystal Structure Determination, University of Göttingen, Germany, 1986.

[33] G.M. Sheldrick, SHELX-93, Program for Crystal Structure Determination, University of Göttingen, Germany, 1993.

[34] (a) D.T. Cromer, J.B. Mann, Acta Crystallogr. Sect. A 24 (1968) 321. (b) D.T. Cromer, D. Liberman, J. Chem. Phys. 53 (1970) 1891. (c) R.F. Stewart, E.R. Davidson, W.T. Simpson, J. Chem. Phys. 42 (1965) 3175.

[35] L. Zsolnai, H. Pritzkow, ZORTEP, ORTEP Program for PC, University of Heidelberg, 1994.